

# Trans-crustal magmatic processes revealed by amphibole breakdown textures at the Quillacas monogenetic volcanic center, Bolivia

L.C. Velázquez Santana<sup>a,\*</sup>, C.L. McLeod<sup>b</sup>, B. Shaulis<sup>c</sup>, M. Loocke<sup>d</sup>, R. Al Gbory<sup>b</sup>

<sup>a</sup> Department of Geological Sciences, University of Colorado at Boulder, 2200 Colorado Ave Boulder, CO 80309, USA

<sup>b</sup> Department of Geology and Environmental Earth Science, Miami University, 250 S. Patterson Avenue Oxford, OH 45056, USA

<sup>c</sup> Trace Element and Radiogenic Isotope Laboratory, University of Arkansas, Fayetteville, AR 72701, USA

<sup>d</sup> Department of Geology and Geophysics, Louisiana State University, Baton Rouge, LA 70803, USA

## ARTICLE INFO

### Keywords:

Amphibole  
Breakdown textures  
Hornblende cumulates  
Magmatic processes  
Monogenetic volcano  
Central Andes

## ABSTRACT

Amphibole exerts a fundamental control on arc magma petrogenesis, differentiation, and the long-term evolution of the arc crust. This study identifies two texturally distinct amphibole populations within andesitic lavas and entrained hornblende cumulates at the Quillacas monogenetic volcanic center in the Eastern Altiplano, Bolivia. Within the hornblendites, all amphiboles are tschermakitic, large ( $\leq 800 \mu\text{m}$ ) with thick, granular reaction rims (avg.  $27 \mu\text{m}$  thickness). In the host andesites, tschermakites are also the dominant amphibole species but are smaller ( $250\text{--}400 \mu\text{m}$ ) with thin, symplectic reaction rims (avg.  $7\text{--}9 \mu\text{m}$  thickness). An intergrowth of symplectic and granular reaction rims is also observed in this population. The amphibole populations within the Quillacas magmatic system also record irregular volumetric decomposition where amphibole is replaced by mineral aggregates of plagioclase, pyroxene, and oxide within the crystal. This suggests the occurrence of a relatively slow reaction between the amphibole and melt trapped in fractures and cleavages during decompression-induced degassing. Geothermobarometry indicates that the hornblende cumulate tschermakites crystallized at P-T conditions ranging from  $467$  to  $598 \pm 12 \%$  MPa and  $945\text{--}991 \pm 22 \text{ }^\circ\text{C}$ . The host andesite tschermakites crystallized at P-T conditions ranging from  $448$  to  $570 \pm 12 \%$  MPa and  $928\text{--}1004 \pm 22 \text{ }^\circ\text{C}$ . These geothermobarometric constraints correspond to depths of  $16\text{--}24 \text{ km}$ , which, within this region of the Central Andean crust, coincides with a regionally extensive low-seismic velocity zone. The texturally distinct amphibole populations imply that a multi-stage trans-crustal magmatic system is likely present beneath the Quillacas volcanic center. In this scenario, a crystal mush zone exists at upper crustal depths where the hornblende cumulate tschermakites initially crystallized. Magma recharge into this mush zone initiated a reaction between hornblende cumulates and the melt which formed the amphibole granular rims. This recharge event also transported the host andesite tschermakites that subsequently developed symplectic rims due to heating and ascent-driven decompression. This study supports the presence of amphibole-dominated mush filters in the upper crust of the Central Andean arc and advances our understanding of amphibole's role in the evolution of arc magmatic systems.

## 1. Introduction

The mineralogy, petrology, and geochemistry of arc volcanic rocks record the complex interplay of magmatic processes that occur at depth (e.g., Cashman et al., 2017; Svoboda et al., 2022). Erupted products therefore have the potential to offer unique insights into the petrogenesis of magmas from source to surface (Humphreys et al., 2006; Kent et al., 2010; Reubi and Blundy, 2009; Straub et al., 2020). Specifically, the crystal cargoes of arc volcanic rocks can 1) provide key constraints

on magmatic storage conditions, 2) identify the origin and cycling of phenocrysts, antecrysts, and xenocrysts, and 3) constrain timescales associated with eruption cycles, crystal residence times, and recharge events (Barboni et al., 2016; Cooper, 2019; Davidson et al., 2005; Ganne et al., 2018; Jackson et al., 2018; Marsh, 2006; Schleicher et al., 2016; Shane and Smith, 2013; Szymanowski et al., 2017; Triantafyllou et al., 2020).

At active continental margins characterized by arc volcanism, amphibole exerts an important control on magma genesis and

\* Corresponding author.

E-mail address: [liannie.velazquezasantana@colorado.edu](mailto:liannie.velazquezasantana@colorado.edu) (L.C. Velázquez Santana).

<https://doi.org/10.1016/j.lithos.2024.107891>

Received 6 September 2024; Received in revised form 26 November 2024; Accepted 27 November 2024

Available online 4 December 2024

0024-4937/© 2024 The Authors. Published by Elsevier B.V. This is an open access article under the CC BY-NC-ND license (<http://creativecommons.org/licenses/by-nc-nd/4.0/>).

subsequent magmatic differentiation (Barber et al., 2021; Davidson et al., 2007; Dessimoz et al., 2012; Kiss et al., 2014; Li et al., 2017; Luo et al., 2024; Velázquez Santana et al., 2020). Numerous studies have investigated the breakdown (reaction) textures of amphibole within magmatic systems and their ability to provide insights into the dynamics of amphibole stability, mineral reactions, and magma ascent times (Buckley et al., 2006; D’Mello et al., 2021; Garcia and Jacobson, 1979; Plechov et al., 2008; Rutherford and Devine, 2003; Rutherford and Hill, 1993). Prior work has established that amphibole instability is driven by several factors including melt degassing during decompression (Kuno, 1950; Garcia and Jacobson, 1979; Rutherford and Devine, 2003; Buckley et al., 2006), temperature increases (Rutherford and Devine, 2003), and/or oxidation of a melt (Garcia and Jacobson, 1979; Murphy et al., 2000; Rutherford and Devine, 2003). Breakdown rims have been well-documented throughout numerous amphibole crystal cargoes at both large, composite arc volcanoes and at small, monogenetic centers (e.g., Devine et al., 1998a, 1998b; D’Mello et al., 2021; Pesquera and Gil-Crespo, 2024; Schaaf et al., 2005; Ureta et al., 2020; Vargas-Arcila et al., 2023). As a result, distinct types of amphibole reaction rims have been identified based on their textural and mineralogical characteristics. Garcia and Jacobson (1979) characterized black rims where microlites of Fe oxides and pyroxene completely or partially replace amphibole. These develop due to oxidation during eruption. Garcia and Jacobson (1979) also described a gabbroic rim type where amphibole is completely or partially replaced by fine- to medium-grained microlites of orthopyroxene, clinopyroxene, plagioclase, and magnetite which results from a decrease in oxygen fugacity in the magmatic system. Murphy et al. (2000) described three types of amphibole reaction rims at the Soufrière Hills volcano, Montserrat: (1) fine-grained (5–30  $\mu\text{m}$ ) aggregates of intergrown pyroxenes, plagioclase, and oxides produced due to amphibole dehydration during ascent; (2) coarse-grained (30–200  $\mu\text{m}$ )

aggregates of intergrown pyroxenes, plagioclase, and oxides that form during an extended recrystallization history; and (3) opaque mineral aggregates that form rims and develop along cleavage planes due to oxidation during eruption. Furthermore, the thickness of amphibole reaction rims has been used as a proxy for magma ascent times in numerous studies (De Angelis et al., 2015; Rutherford and Devine, 2003; Rutherford and Hill, 1993). However, defining the timescales of magma ascent is challenging due to several factors, including the initial depth from which magma begins its ascent, fluctuations in ascent rates, and the variable parameters that affect amphibole stability (D’Mello et al., 2021).

In this study, we investigated the petrogenesis of two texturally distinct amphibole populations within rare hornblende cumulates and their amphibole-bearing Plio-Pleistocene volcanic host rocks. This unique petrological association occurs at the andesitic Quillacas monogenetic center located in the back-arc region of the Bolivian Altiplano, Central Andes (Fig. 1). The mineralogy and geochemistry of the hornblende cumulates was previously investigated by Velázquez Santana et al. (2020). Here, we report *in-situ* major and trace element geochemistry for the amphibole populations in the andesites and hornblende cumulates, a textural analysis of amphibole breakdown rims, and an assessment of P-T conditions within the Quillacas magmatic system from source to surface. The aim of this study was therefore twofold: 1) to determine whether the amphibole populations originated from multiple magma batches and evaluate if one or multiple sources were involved and 2) to assess whether there were multiple storage zones within the arc crust where amphibole was fractionating, mobilizing, and/or stalling. Collectively, this dataset aims to advance our understanding of the role of amphibole in the evolution of arc magmatic systems.

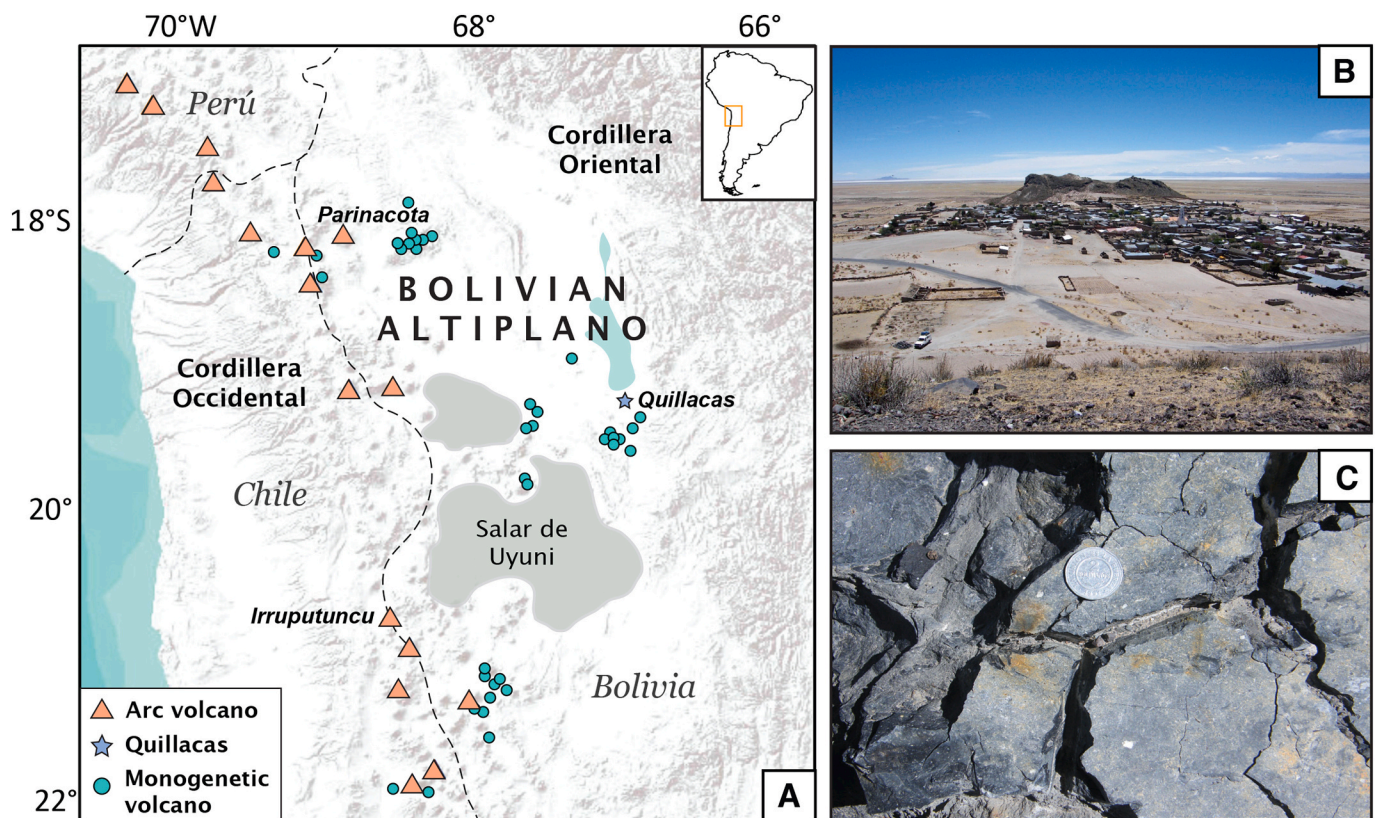


Fig. 1. (a) Terrain map of Central Andean Volcanic Zone (CVZ) from 16 to 22°S including the location of the Quillacas volcanic center which is the focus of this study. The inset map shows the location of the CVZ within the Andean Cordillera of South America. Map is modified from Velázquez Santana et al. (2020) (b) Image of Quillacas volcanic center and surrounding Quillacas town. (c) Field image of Quillacas andesite, 2 Bolivianos coin used for scale.

## 2. Geological background

The Central Volcanic Zone (CVZ) of the Central Andes, South America extends from 16 to 22°S and is bound by regions of volcanic quiescence to the north and south, and to the west by the Interandean Zone (i.e., tectonomorphic transition zone between the Eastern Andean Cordillera and the low-elevation valleys). Magmatism and volcanism in the CVZ are driven by the subduction of the Nazca Plate beneath the South American Plate and are expressed at the surface as an extensive volcanic arc front characterized by predominantly andesitic composite volcanoes (Zandt et al., 1994; Beck and Zandt, 2002; Wörner et al., 2018; Fig. 1). Magmatism is also expressed as monogenetic volcanism in the behind- and back-arc regions extending for ~180 km east of the CVZ arc front (Davidson and de Silva, 1992, 1995). This type of volcanism is prevalent across the Bolivian Altiplano between 18 and 20°S. At these latitudes, due to the continental crustal basement extending to c. 75 km in depth, magma ascent driven by buoyancy is difficult to reconcile (Ward et al., 2016; Göğüş et al., 2022). It is therefore highly likely that the crustal thickness significantly impedes the ascent of mantle-derived melts (Ward et al., 2016; Göğüş et al., 2022). An explanation for back-arc volcanism in this region was proposed by Marrett and Emerman (1992) which related the spatiotemporal occurrence of monogenetic volcanism to regional fault activity in the Central Andes. This led to the suggestion that the distribution of monogenetic volcanism in the back-arc region is intricately related to fault activity with fault planes acting as conduits for ascending mantle-derived melts. Fault kinematic studies have described two distinct phases of deformation styles from the Miocene-Pliocene into the Quaternary (Cladouhos et al., 1994; Marrett and Emerman, 1992). The older phase (the Quechua phase, 21.5 to 12.5 Ma after Mégard et al., 1984) is characterized by a regime of NW-SE shortening on dip-slip faults and vertical extension. A younger phase occurred in a strike-slip regime with NE-SW to E-W shortening and NW-SE and N-S horizontal extension. This change in crustal stress regime promoted the vertical intrusion of mantle-derived magma and drove surface eruptions during the end of the Pliocene (c. 2.6 Ma). This event spatially and temporally correlates with the eruption of monogenetic

volcanic centers across the Bolivian Altiplano back-arc and behind arc regions, which range in age from Pliocene to Pleistocene, and in composition from basaltic andesite to dacite (Davidson and de Silva, 1992, 1995; Marrett and Emerman, 1992). Here we focus on the c. 1.4 Ma Quillacas monogenetic volcanic center which is the easternmost center located in the Bolivian Altiplano (Fig. 1). The lavas erupted from the Quillacas center are host to a suite of hornblende cumulates (Velázquez Santana et al., 2020) and a suite of petrologically diverse, partially melted crustal xenoliths (McLeod et al., 2012, 2013). In this study, we focus on three samples associated with the Quillacas volcanic center: one hornblende, and two host andesites (Fig. 2).

## 3. Methods

### 3.1. Scanning electron microscopy (SEM)

Back-scatter electron (BSE) images were acquired on a Zeiss Supra 35 Variable Pressure Field Emission Gun-Scanning Electron Microscope (VP FEG-SEM) at Miami University's Center for Advanced Microscopy and Imaging (CAMI). Images were captured using an accelerating voltage of 25 KeV, a working distance between 6 and 10 mm, through a 120  $\mu\text{m}$  aperture at variable magnifications.

### 3.2. Electron probe microanalysis (EPMA)

Major element analysis of selected amphiboles was conducted via EPMA on a JEOL JXA-8230 electron MicroProbe in the Chevron Geomaterials Characterization Lab, Department of Geology and Geophysics at Louisiana State University. A 15 kV accelerating potential, a 20 nA beam current, and a 5  $\mu\text{m}$  spot size were used. Elemental abundances are reported in wt% oxide in the supplementary Excel data table found in Database: Mendeley: 10.17632/45bhdjbnf.

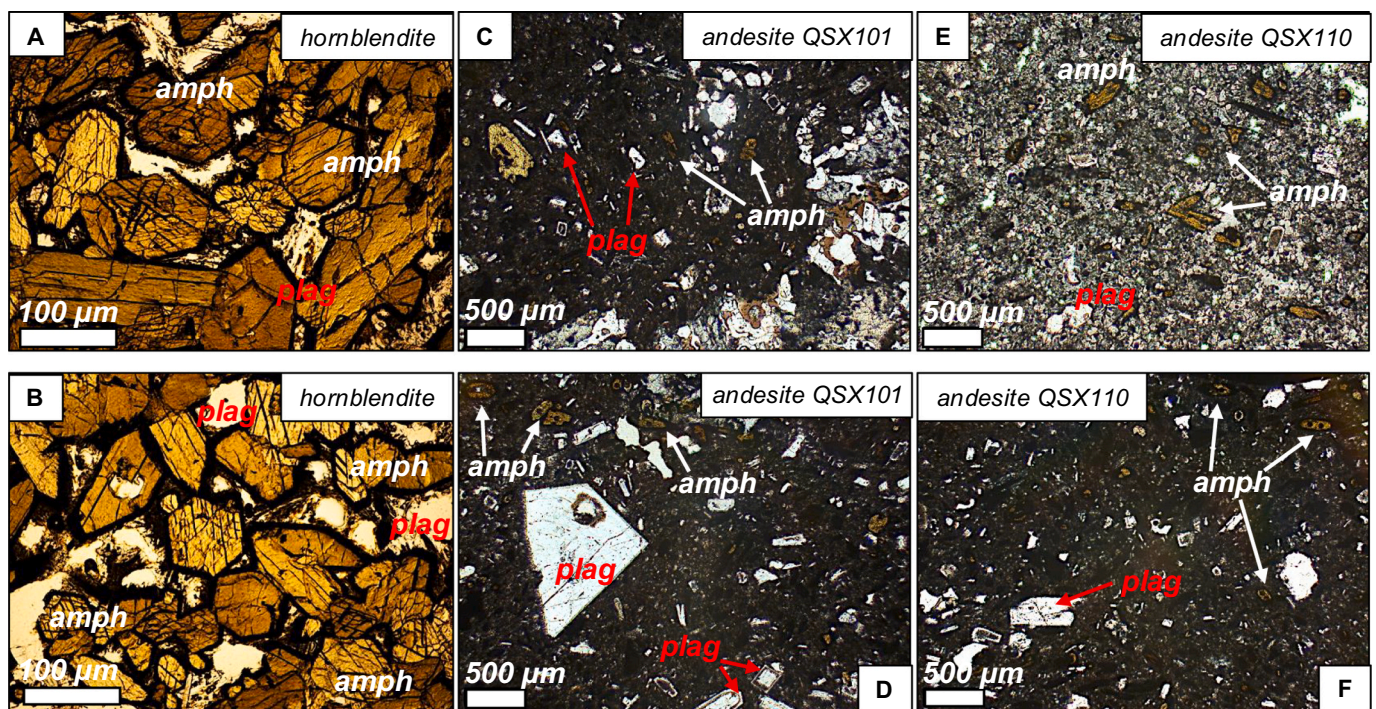


Fig. 2. Plane-polarized light (PPL) images of studied samples. (a-b) Hornblende (QNMIC) photomicrographs in PPL. (c-d) Host andesite (BC10QXSX101) photomicrographs in PPL. (e-f) Host andesite (BC10QXSX110) photomicrographs in PPL. Abbreviations: amph – amphibole, plag – plagioclase.

### 3.3. Laser ablation-inductively coupled plasma-mass spectrometry (LA-ICP-MS)

Trace element analysis of selected amphiboles was conducted via LA-ICP-MS on a Thermo-iCAP Q quadrupole mass spectrometer coupled with a New Wave/ESI 193 nm laser ablation system at the University of Arkansas Trace Element and Radiogenic Isotope Laboratory (TRAIL). Laser ablation was performed using a 50  $\mu\text{m}$  laser spot diameter. For all analyses, the following settings were applied: 10 Hz repetition rate over 20s, laser fluence at  $\sim 4.3 \text{ J/cm}^2$ , and a He carrier gas flow rate of 0.8 L/min. Elemental abundances are reported in ppm in the supplementary Excel data table found in Database: Mendeley: [10.17632/45bhdjbdnf](https://doi.org/10.17632/45bhdjbdnf).

## 4. Petrography

### 4.1. Hornblende (sample QNMIC)

One representative hornblende sample (QNMIC; Fig. 2a-b) was chosen for this study due to its geochemical, mineralogical, and textural equivalence within the entire suite (Velázquez Santana et al., 2020). The hornblendites, generally ranging from 3 to 5 cm in size as hand samples, were collected as individual cumulates (weathered out) and as inclusions within the andesite host (McLeod et al., 2012). While the Quillacas lavas contain relatively abundant crustal xenoliths (5–10 %; McLeod et al., 2013), the hornblendites are comparatively rare. The mineral assemblage of the hornblendites is characterized by medium-coarse grained amphiboles (>90 %), plagioclase feldspar ( $\sim 8$  %), and minor (titano)magnetite alongside accessory apatite (Velázquez Santana et al., 2020; Fig. 2a-b). Specifically, the hornblendites are mesocumulates with amphiboles as the cumulus phase and plagioclase, minor (titano)magnetite, and accessory apatite as the dominant interstitial (groundmass) phases. Amphiboles exhibit a euhedral habit with all grains associated with opaque (opacitic) rims. Their sizes range in size

from 700 to 800  $\mu\text{m}$  while some grains ( $\sim 15$ –20 %) exceed 1 mm (Velázquez Santana et al., 2020; Fig. 3a).

### 4.2. Andesitic host lavas (samples BC10QXSX101 and BC10QXSX110)

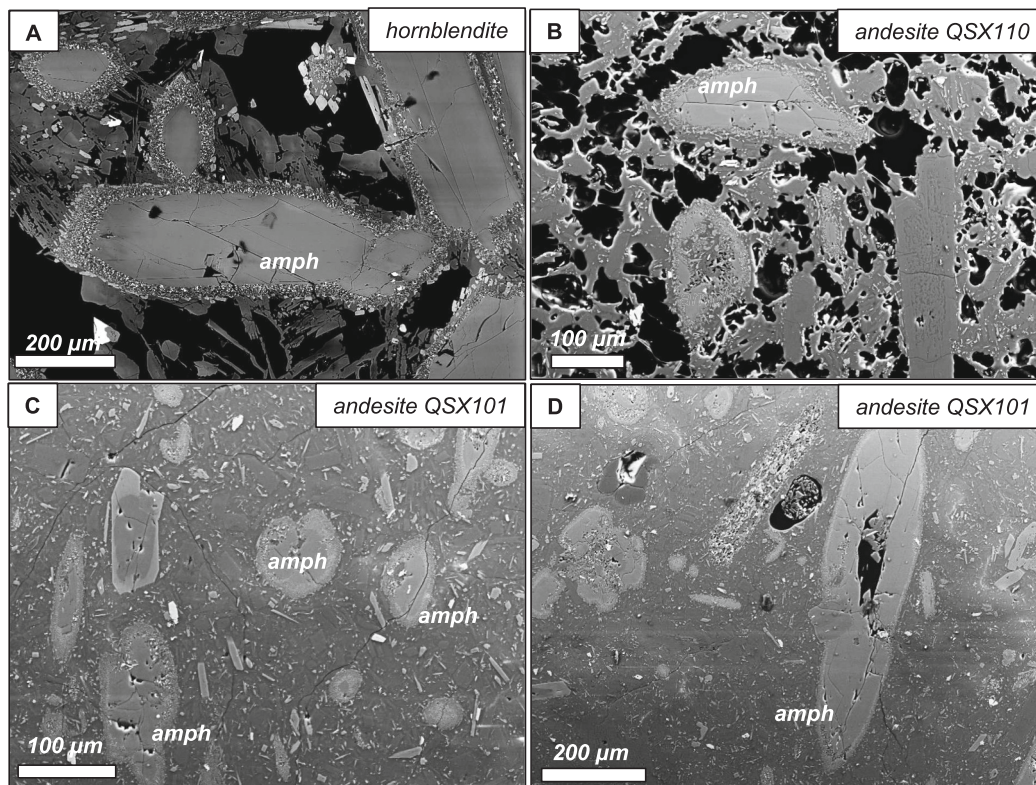
Sample BC10QXSX101 is a porphyritic andesite with a fine-grained groundmass that constitutes  $\sim 70$ –75 % of the sample. Its mineral population includes plagioclase feldspar, amphibole, with minor biotite and clinopyroxene, and rare olivine (Fig. 2c-d). Amphiboles within this sample are generally subhedral to anhedral and range in size between 10 and 400  $\mu\text{m}$ , with some grains exceeding 400  $\mu\text{m}$  (Fig. 3b-d). Amphiboles show polycrystalline, opaque rims and weak chemical zoning. Plagioclase feldspar grains are euhedral to subhedral. A rare olivine crystal clots were also identified in this sample.

Sample BC10QXSX110 is an aphanitic andesite with a groundmass mostly composed of plagioclase feldspar, amphibole, biotite, and pyroxene (Fig. 2e-f). Amphiboles within this sample are euhedral to subhedral and range in size between 10 and 700  $\mu\text{m}$ . All amphiboles show opaque rims, and some are zoned (Fig. 3b). A few euhedral to subhedral grains of plagioclase as well as subhedral to anhedral, embayed quartz xenocrysts are present in this sample.

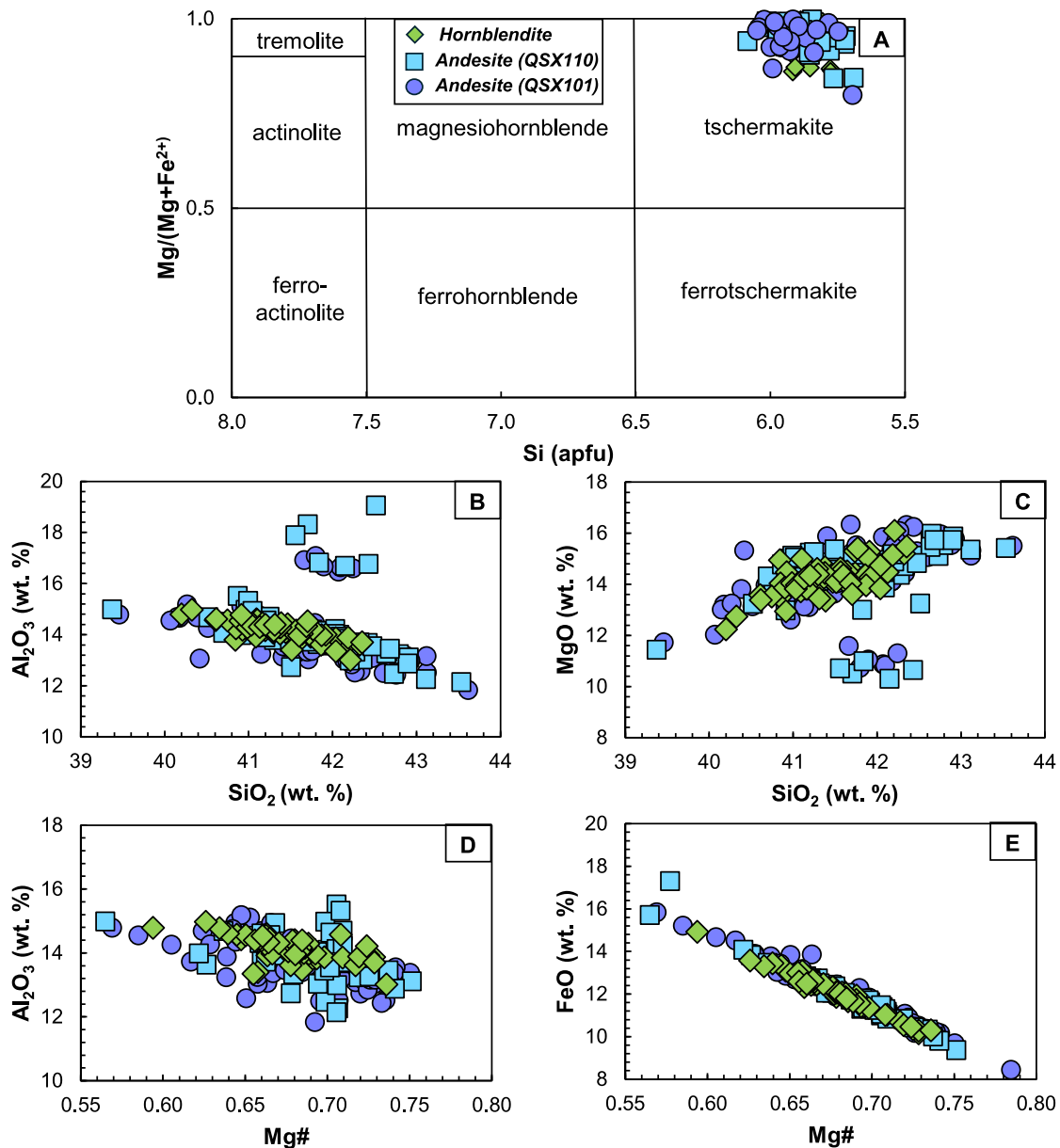
## 5. Results

### 5.1. Amphibole chemistry

Major element data for amphiboles within the hornblende and Quillacas andesites were acquired via electron probe microanalysis (EPMA). The major element chemistry of the amphibole populations in the hornblendites and andesites is consistent with tschermakite, a high-Ca amphibole (Fig. 4a; Leake et al., 1997). A negative correlation is observed between wt%  $\text{Al}_2\text{O}_3$  and  $\text{SiO}_2$  with the andesite amphiboles demonstrating a slightly wider range in  $\text{SiO}_2$  contents (39–44 wt%;



**Fig. 3.** (a) Scanning electron microscope-backscattered electron (SEM-BSE) image of hornblende. (b) SEM-BSE image of QL andesite BC10QXSX110. (c-d) SEM-BSE images of andesite BC10QXSX101. Abbreviations: amph – amphibole.



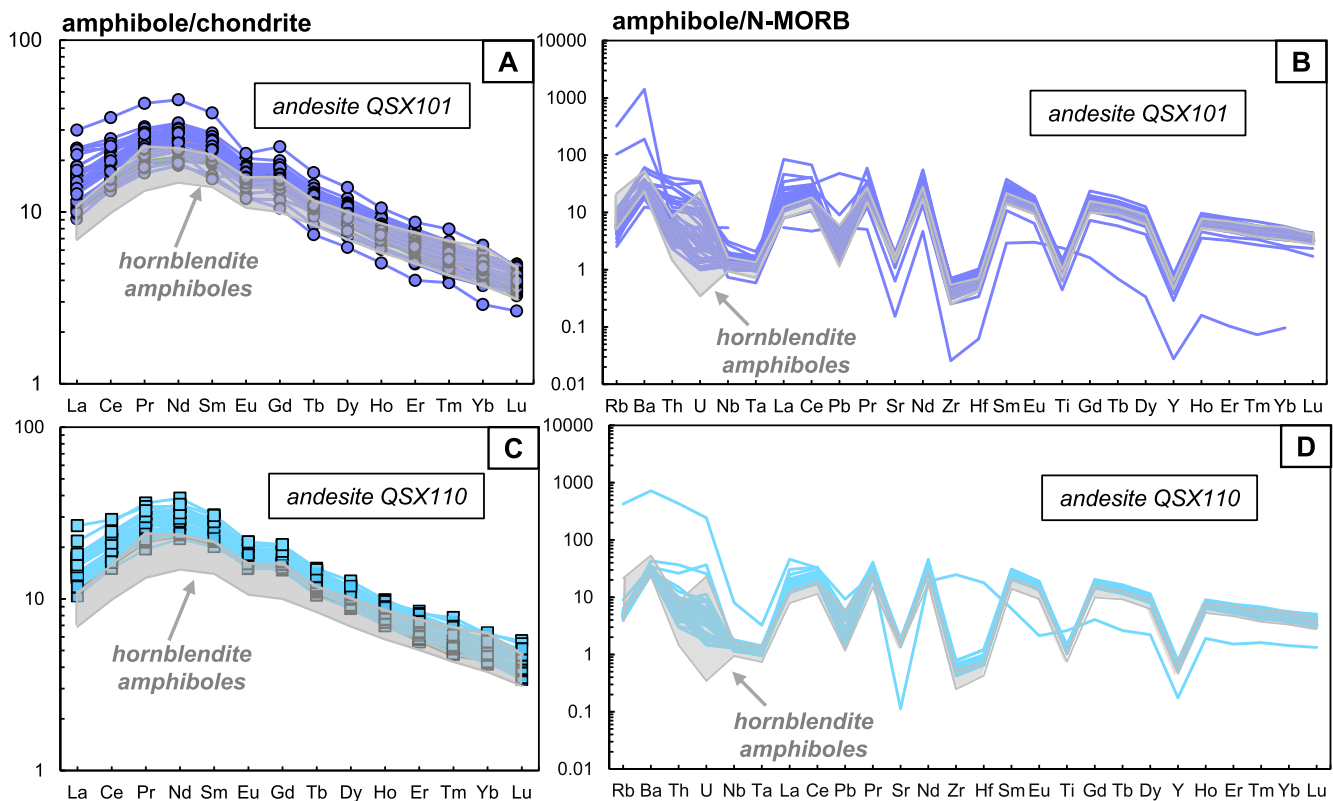
**Fig. 4.** (a) Amphibole classification diagram for Ca-amphiboles based on Leake et al. (1997). (b) Amphibole major element oxide composition diagram for  $\text{Al}_2\text{O}_3$  vs.  $\text{SiO}_2$  (wt%) (c)  $\text{MgO}$  vs  $\text{SiO}_2$  (wt%). (d)  $\text{Al}_2\text{O}_3$  vs  $\text{Mg\#}$  ( $\text{Mg}/\text{Fe}^{3+}+\text{Mg}$ ). (e)  $\text{FeO}$  vs.  $\text{Mg\#}$ .

Fig. 4b). A positive correlation is observed between wt%  $\text{MgO}$  and  $\text{SiO}_2$  (Fig. 4c). Using  $\text{Mg\#}$  ( $\text{Mg}/\text{Fe}^{3+}+\text{Mg}$ ) as a differentiation index, a negative correlation is observed between wt%  $\text{Al}_2\text{O}_3$  and  $\text{Mg\#}$  (Fig. 4d). A strong negative correlation is observed between wt%  $\text{FeO}$  and  $\text{Mg\#}$  which is expected due to the coupled substitution of  $\text{Fe}^{2+}$  and  $\text{Mg}^{2+}$  in the amphibole crystal lattice (Fig. 4e). Overall, the chemical compositions of the amphibole populations in the hornblendite cumulate and the host andesites are generally tightly clustered with more chemical variability present within the andesite amphibole population.

Trace element data for amphiboles within the Quillacas andesites was acquired via laser ablation inductively coupled plasma mass spectrometry (LA-ICP-MS). Amphibole trace element data for Quillacas hornblendites is reported in Velázquez Santana et al. (2020). Amphiboles from both the andesites and hornblendite samples exhibit signatures typical of amphibole in subduction settings. Amphiboles from sample BC10QSX101 demonstrate moderate light rare earth element (LREE) depletion ( $\text{La}_N/\text{Sm}_N$ : 0.47–2.27), enrichment in middle rare earth elements (MREE) ( $\text{Sm}_N/\text{Dy}_N$ : 2.09–2.96), and heavy rare earth

element (HREE) depletion ( $\text{Dy}_N/\text{Lu}_N$ : 1.91–2.91; Fig. 5a). Negative Eu anomalies ( $\text{Eu}/\text{Eu}^*$ ) are consistently observed and range from 0.73 to 0.94 ( $n = 42$ ; Fig. 5a). In addition, the amphiboles from this sample display enrichment in large ion lithophiles (LILEs), particularly Rb and Ba, compared to N-MORB, alongside depletions in Nb and Ta, indicating a subduction-related signature (Fig. 5b). A negative Zr is present, as expected, given that the partition coefficient ( $D_{Zr}$ ) of Zr in amphibole is typically less than 1 which favors depletion. A negative Ti anomaly is also observed, likely due to Ti partitioning into co-crystallizing phases such as titanite, ilmenite, or magnetite, which preferentially incorporate Ti, reducing its availability during amphibole crystallization. For comparison, trace element patterns from the hornblendite amphiboles overlap with those from the Quillacas andesites. The main difference is a more pronounced negative U anomaly in the hornblendite amphiboles, which may result from variable redox conditions or source heterogeneity during crystallization (Fig. 5b).

Amphiboles from sample BC10QSX110 also show moderate LREE depletion ( $\text{La}_N/\text{Sm}_N$ : 0.51–0.96), MREE enrichment ( $\text{Sm}_N/\text{Dy}_N$ :



**Fig. 5.** (a) Amphibole chondrite-normalized rare earth element (REE) diagram for andesite BC10QXSX101. (b) Amphibole N-MORB-normalized extended trace element diagram for andesite BC10QXSX101. (c) Amphibole chondrite-normalized rare earth element (REE) diagram for andesite BC10QXSX110. (d) Amphibole N-MORB-normalized extended trace element diagram for andesite BC10QXSX110. Grey field represents trace element composition ranges for amphiboles in Quillacas hornblendites from Velázquez Santana et al. (2020). Chondrite normalizing values from Nakamura (1974). N-MORB normalizing values from Sun and McDonough (1989).

2.18–2.62), and HREE depletion ( $Dy_N/Lu_N$ : 1.63–2.78; Fig. 5c). Negative Eu anomalies are also recorded within this sample and range from 0.48 to 0.93 ( $n = 37$ ; Fig. 8b). When compared to the Quillacas hornblendites, LREE values for the andesites show a slightly greater variability but still overlap with the general range of the Quillacas samples (Fig. 5c; Velázquez Santana et al., 2020). The MREE enrichment and HREE depletion observed in the andesites are also consistent with values reported for the hornblende amphiboles. The negative Eu anomalies show a slightly larger range relative to the hornblendites and are consistent with the fractionation of plagioclase. Additionally, as shown in Fig. 5d, amphiboles from sample BCQXSX110 exhibit almost identical trace element patterns to those in sample BC10QXSX101, with relative LILE enrichment, Nb—Ta, Zr, and Ti depletion.

## 5.2. Amphibole breakdown textures

### 5.2.1. Reaction rims

Amphiboles within the Quillacas hornblendites and andesites commonly exhibit breakdown textures associated with melt reaction or volumetric breakdown. The most observed reaction rims in the Quillacas amphibole suite are ‘opacite rims’ (Plechov et al., 2008), which appear black under plane polarized light (Fig. 2). The reaction rims observed in the hornblende cumulates are coarse-grained, equant, and exhibit thicknesses averaging 27.25  $\mu\text{m}$  (Fig. 6). Within the andesites, the reaction rims are finer grained with thicknesses averaging 7–9  $\mu\text{m}$  (Fig. 6). The rims of both cumulate and andesite amphiboles are mineralogically equivalent with a three-phase mineral assemblage described as gabbroic that consists of varying amounts of Fe-Ti oxides, plagioclase feldspar, and pyroxene (refer to Kuno, 1950; Garcia and Jacobson, 1979; Rutherford and Hill, 1993; De Angelis et al., 2015). Based on textural

differences, three types of reaction rims are observed in the Quillacas amphiboles:

1. **Detached rims:** Detached rims are commonly found in both the hornblende and andesite amphiboles independent of the presence of symplectic or granular rims. These rims were observed in all the studied amphiboles in the hornblende and andesites. The rims consist of pyroxene grains (1–10  $\mu\text{m}$  in hornblendites, 1–5  $\mu\text{m}$  in andesites) that appear to be suspended in their carrier melt and are aligned parallel to sub-parallel to the amphibole crystal faces (Fig. 6a-d). Their formation is attributed to a minor but significant increase in temperature within amphibole’s stability field (Rutherford and Devine, 2003). D’Mello et al. (2021) proposed that this can occur due to melt interaction where amphibole begins to dissolve and then grows into clinopyroxene microlites at the boundary of the crystal. This process initiates amphibole breakdown when the crystal is entrained in an ascending, hot, low-viscosity melt (D’Mello et al., 2021).
2. **Symplectic rims:** Found only in the andesites, these rims are characterized by intergrown crystals of plagioclase + pyroxene + oxide that are perpendicular to the crystal face (Fig. 6b-d). These rims are present in all the studied amphiboles in the andesites. They are observed closest to the unaltered amphibole and are not present when the crystal is not in direct contact with the glass. The rims are generally thicker at the crystal edges compared to along the face. It has been suggested that to generate this rim type a magmatic reaction of an unstable amphibole with its carrier magma is essential (D’Mello et al., 2021). This formation mechanism is consistent with textural observations of the Quillacas amphiboles where there is no

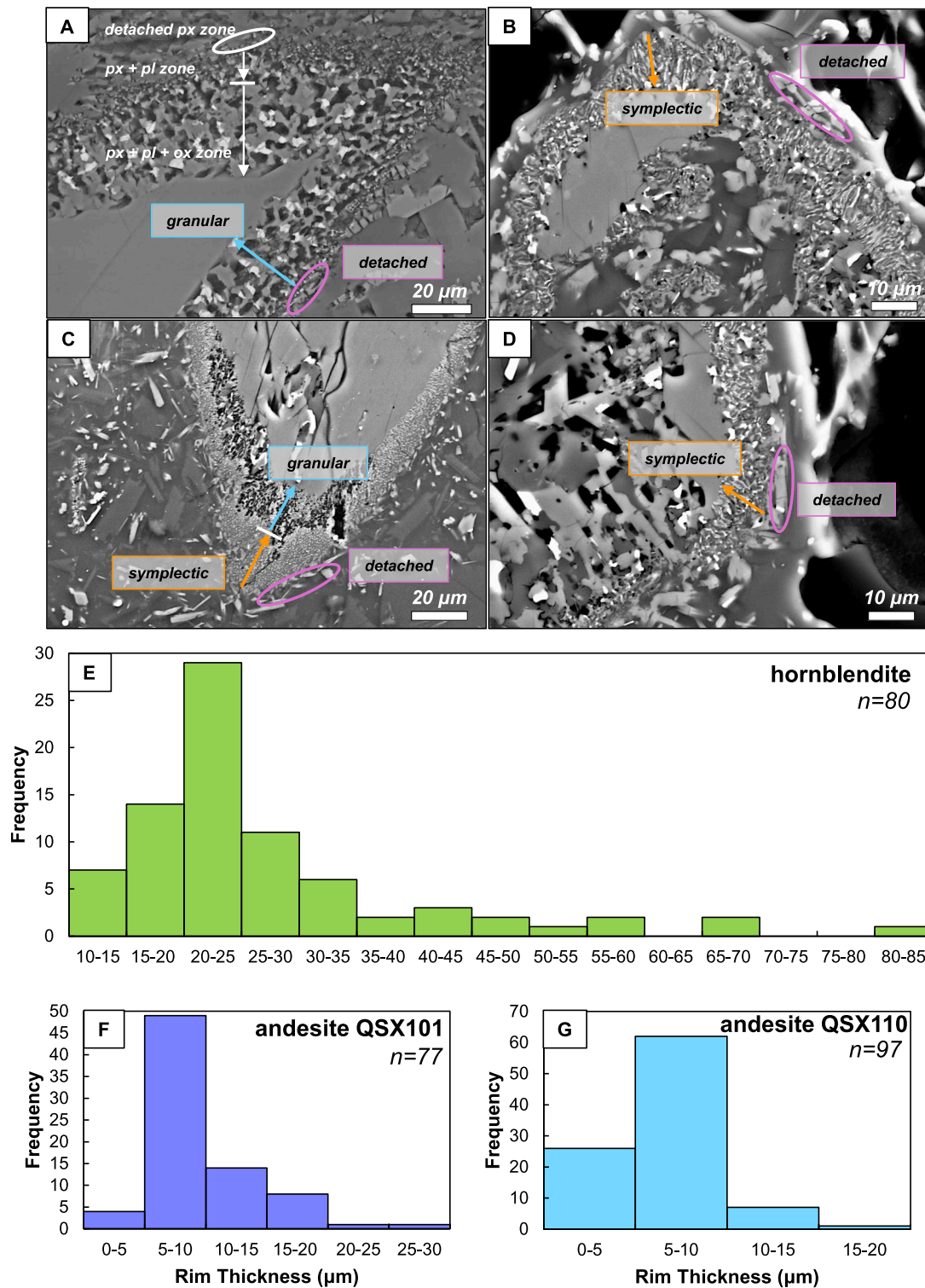


**Fig. 6.** (a) SEM-BSE image of granular and detached reaction rims within the hornblende. Three zones are identified within the rim: (1) pyroxene + plagioclase + oxide, (2) pyroxene + plagioclase, and (3) pyroxene detached rim. (b) BSE image of amphibole symplectic and detached reaction rims within andesite sample BCQXSX101. (c) BSE image of intergrowth of symplectic and granular reaction rim within andesite sample BC10QXSX110. (d) BSE image of symplectic and detached reaction rims in andesite sample BC10QXSX110. Abbreviations: plag – plagioclase feldspar, px – pyroxene, ox – oxide. Histograms of reaction rim thickness measurements for (e) hornblende amphiboles ( $n = 80$ ), (f) andesite (BC10QXSX101) amphiboles ( $n = 77$ ), and (g) andesite (BC10QXSX110) amphiboles ( $n = 97$ ).

rim formation in areas where no apparent contact with their carrier melt has occurred (Fig. 7).

- Granular rims:** These rims, observed as the sole type in the hornblendites, consist of anhedral aggregates of plagioclase + pyroxene + oxide ( $>1 \mu\text{m}$ ; Fig. 6a). In addition to forming around the faces of the

amphiboles, they also sometimes form along cleavage planes and fractures of the crystals. These rims were observed in all the amphiboles in the hornblendites. Intergrowths of both granular and symplectic rims are observed in the andesite amphiboles. This intergrowth of both rim types is a minor occurrence, only observed in

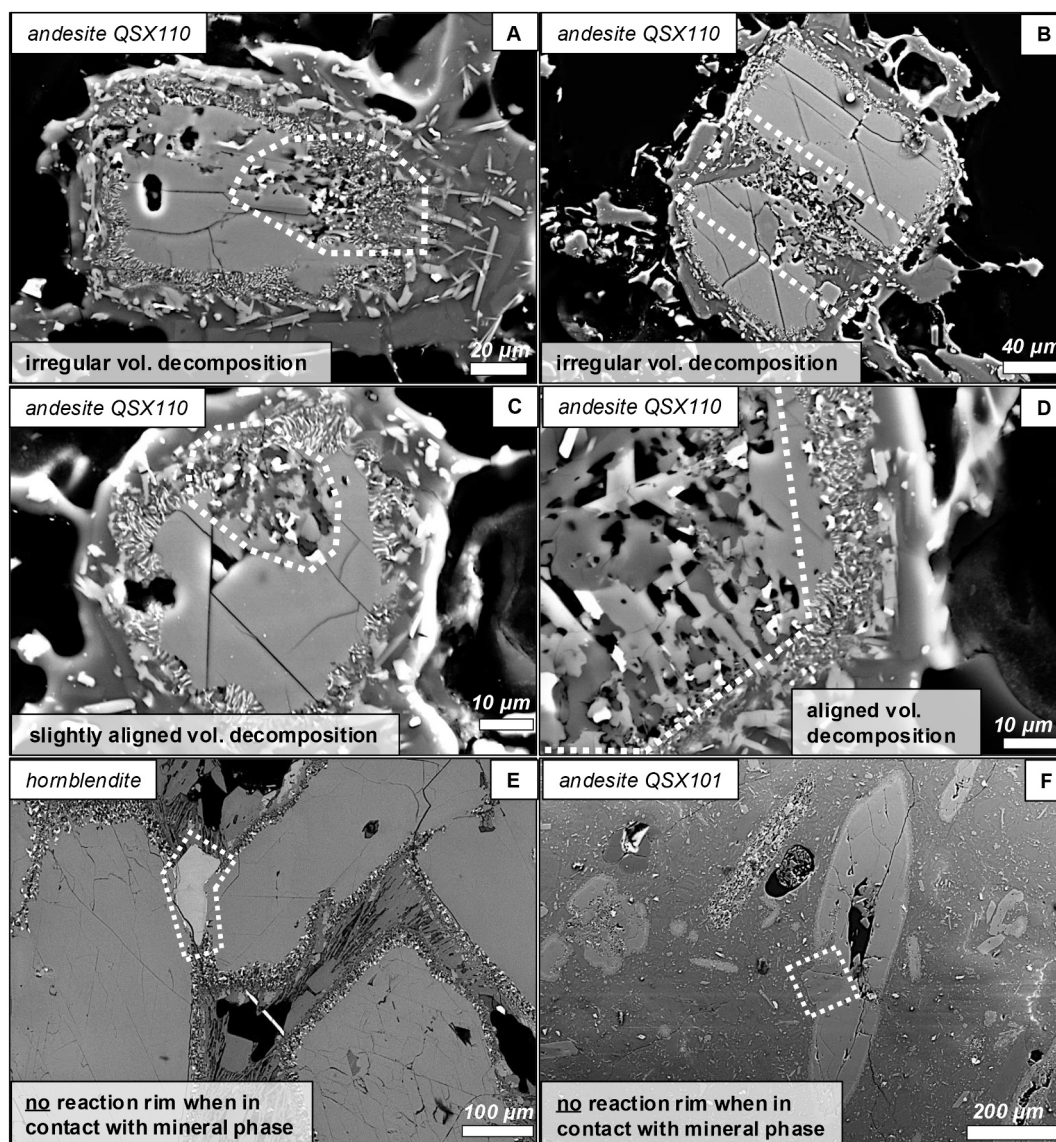


**Fig. 7.** SEM-BSE images of volumetric decomposition observed in hornblende and andesite tschermakitic amphiboles. (a) Region of irregular volumetric decomposition in andesite amphibole occupying a fracture in the amphibole. (b) Region of irregular volumetric decomposition in the center of an amphibole crystal within the andesite. (c) Region of slightly aligned volumetric decomposition in association with reaction rims. (d) Rare aligned volumetric decomposition intersecting the reaction rim in andesite. Example in the (e) hornblende and (f) andesite of the absence of reaction rim formation when the amphibole is in contact with another mineral phase rather than the melt.

~10 % of the studied amphiboles in the andesites. In this case, granular rims can either replace parts of the symplectic rims along crystal faces or occur along cleavage planes and/or fractures. This occurrence has also been observed in Taranaki amphiboles from New Zealand (D’Mello et al., 2021). The granular rims are also absent when the amphibole is in contact with another mineral phase rather than the melt (Fig. 7). The granular rims in the hornblende amphiboles are consistent with the formation mechanism proposed by Plechov et al. (2008) where the following sequence of zones is defined: pyroxene + plagioclase + Ti-magnetite in contact with the amphibole, followed by a pyroxene + plagioclase zone, and a pyroxene zone in contact (detached rims) with the melt (Fig. 6a).

### 5.2.2. Volumetric decomposition

Another common breakdown feature in the Quillacas amphibole populations is volumetric decomposition where amphibole is replaced by aggregates of plagioclase, pyroxene, and oxide within the crystal (Plechov et al., 2008; Fig. 7a-d). These regions may intersect with the

reaction rim or be entirely enclosed within the crystal without any clear contact with the groundmass. The predominant type throughout the Quillacas amphiboles is irregular volumetric decomposition based on the orientation and mineral composition. In this case, subhedral to anhedral grains of plagioclase + pyroxene + oxide occupy areas within the amphibole crystal with no clear alignment. At times, the volumetric decomposition breakdown texture is observed to intersect the reaction rims (Fig. 7a-d). A potential mechanism for the formation of this breakdown has been proposed by D’Mello et al. (2021) where amphibole slowly reacts with melt trapped in its fractures and cleavages during decompression-induced degassing.

### 5.3. Amphibole P-T calculations

Amphibole major element compositions are used to evaluate the pressure (P) and temperature (T) conditions of amphibole crystallization within the Quillacas magmatic system. In this study, we apply the Amp-TB2 thermobarometer from Ridolfi (2021) to assess the P-T conditions of

amphibole crystallization. The Amp-TB2 model is based on experimental data and determines P-T conditions for Mg-rich calcic amphiboles that crystallized in equilibrium with calc-alkaline or alkaline melts (Ridolfi, 2021). More details regarding the parameters and uncertainties of this mineral thermobarometer can be found in Ridolfi (2021). The calculated temperatures for the Ca-amphiboles from all three samples that fit the Amp-TB2 thermobarometer error boundaries ( $n = 107$ , accepted) are tightly constrained to temperatures ranging between 928 and  $1004 \pm 22$  °C and pressures between 448 and  $598 \pm 12$  % MPa (Fig. 8a). All accepted values returned from the model were associated with tschermakite amphibole species (Ridolfi, 2021; Fig. 4a). Ca-amphiboles that were not accepted by Amp-TB2 ( $n = 75$ ) were due to composition-related incompatibilities with the model. Notably, the Amp-TB2 calibration is specific to Mg-rich calcic amphiboles and some amphiboles particularly those in the andesites, show a broad range of Mg contents: 10–15 wt%. Our results suggest that Amp-TB2 performs optimally for calcic amphiboles with corresponding Mg contents at 12–15 wt%. For the hornblende amphiboles specifically, calculated P values range from 467 to 598 MPa ( $\pm 12$  %) while calculated T values range from 945 to 991 °C ( $\pm 22$ ;  $n = 56$ ; Fig. 8a). For the BC10QSX110 andesite, the calculated P values range from 448 to 570 MPa ( $\pm 12$  %) while T values range from 963 to 1004 °C ( $\pm 22$ ;  $n = 20$ ; Fig. 8a). For the BC10QSX101 andesite, calculated P values range from 458 to 557 MPa ( $\pm 12$  %) while T values range from 928 to 999 °C ( $\pm 22$ ;  $n = 31$ ; Fig. 8a). From these P estimates, a depth range of 16–24 km within the upper Central Andean crust is estimated for the formation of the Quillacas amphibole populations. Additionally, the  $H_2O_{melt}$  (wt%) content of the amphiboles within the studied suite has been determined using the Ridolfi (2021) Amp-TB2 thermobarometer (Fig. 8b). Results yielded  $H_2O_{melt}$  (wt%) contents for the hornblende cumulates which range from 5.1 to 7.5 (Fig. 8b; five outliers excluded). For the BC10QSX110 andesite, amphibole  $H_2O_{melt}$  (wt%) contents range from 4.5 to 7.5 (Fig. 8b; one outlier excluded) which is similar to those determined for the BC10QSX101 andesite which range from 4.7 to 7.5 (Fig. 8b; one outlier excluded).

## 6. Discussion

### 6.1. Amphibole stability within the Quillacas magmatic system

Determining the P-T conditions of amphibole stability is crucial for understanding the implications of the range of breakdown features observed within the Quillacas andesites and the entrained hornblende cumulates. Previous experimental studies have demonstrated the utility of amphibole compositions to quantify pre-eruptive conditions including temperature, pressure, oxygen fugacity, and water content (Molina et al., 2015; Ridolfi, 2021; Ridolfi and Renzulli, 2012). Here we apply the Ridolfi (2021) Amp-TB2 thermobarometer which uses amphibole-only compositions to estimate P-T conditions with a low uncertainty ( $12$  % MPa,  $\pm 22$  °C). The P-T conditions for all studied Quillacas amphiboles are tightly constrained to  $928$ – $1004 \pm 22$  °C with corresponding pressures between 448 and  $598 \pm 12$  % MPa. When correlating P estimates to depth, a range of 16–24 km is estimated for the Quillacas amphiboles, consistent with upper continental crustal depths beneath the Eastern Cordillera, Central Andes (Fig. 8a). This therefore suggests a common origin and storage zone for both the cumulate and andesite amphiboles within the Quillacas magmatic system. Furthermore, this depth estimate strongly correlates with a low-seismic velocity zone ( $3.2$  Vs km/s; refer to Fig. 12 in Gao et al., 2021) observed at 20–25 km depth at  $19^\circ$ S,  $66^\circ$ W in the Eastern Cordillera, Bolivia. This geophysical observation therefore independently validates the P (and depth) estimates obtained from amphiboles in this study and corroborates the presence of partial melts in this area related to back-arc monogenetic volcanism.

Despite the utility of the Ridolfi (2021) Amp-TB2 thermobarometer for estimating P-T conditions, a careful examination of elemental trends in the Quillacas amphibole compositions reveals limited correlations between  $^{IV}Al$  and other key cations (e.g.  $^{VI}Al$ , Ti,  $A(Na + K)$ , and Ca; Fig. 9), which are typically indicative of P- and T-dependent substitution mechanisms (Anderson and Smith, 1995; Hammarstrom and Zen, 1986; Helz, 1982). The absence of these trends in the Quillacas amphibole

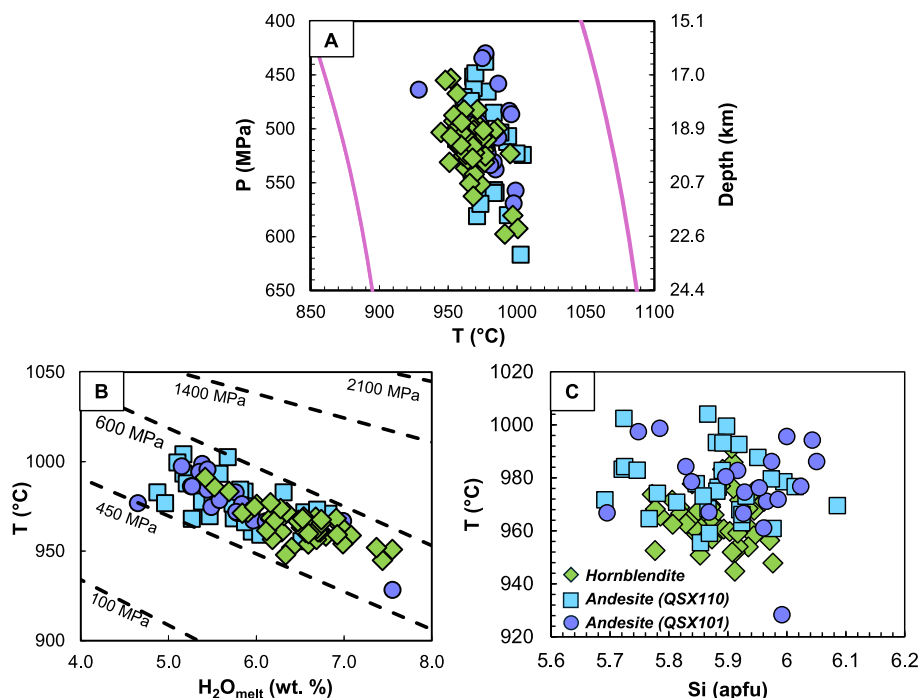


**Fig. 8.** (a) Pressure (P), temperature (T), and depth (D) calculations for amphiboles using the Ridolfi (2021) Amp-TB2 thermobarometer. The pink curves delineate the model's validity and uncertainties of the method. (b) T (°C) vs.  $H_2O$  melt (wt%) for amphiboles within the hornblende and two host andesites. (c) T (°C) vs. Si (apfu) for amphiboles within the hornblende and the two host andesites. Uncertainties associated with the Ridolfi (2021) Amp-TB2 thermobarometer are  $P \pm 12$  %,  $T \pm 22$  °C, and  $H_2O$  in the melt  $\pm 14$  %. (For interpretation of the references to colour in this figure legend, the reader is referred to the web version of this article.)

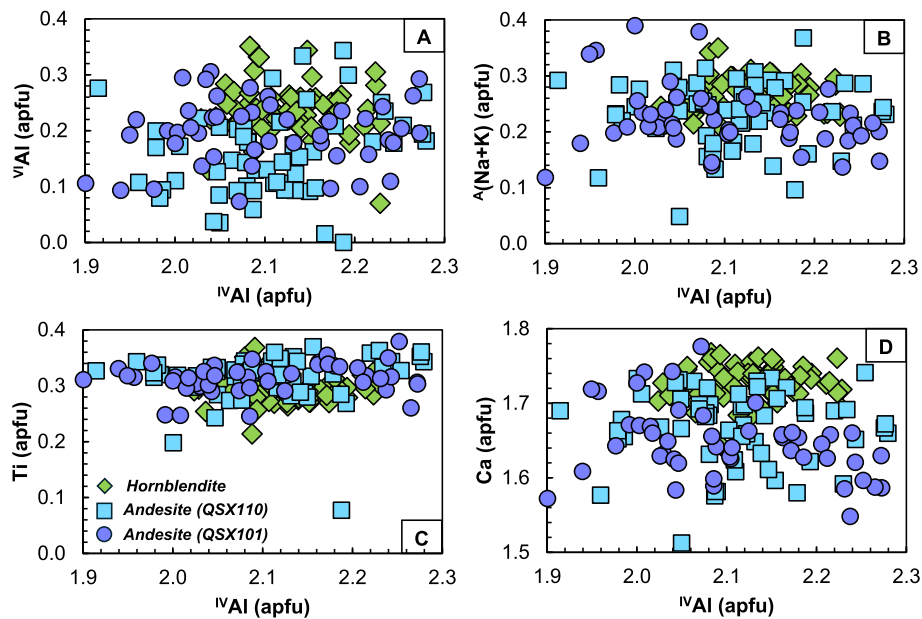


Fig. 9. Amphibole compositions in studied samples shown as site-specific cation concentrations.  $^{IV}Al$  (apfu) versus (a)  $^{VI}Al$  (apfu) (b)  $A(Na + K)$  (c) Ti (apfu) (d) Ca (apfu).

population data suggests that amphibole compositions may be more strongly influenced by melt composition or rapid crystallization under non-equilibrium conditions rather than stable pressure and temperature alone (Krawczynski et al., 2012; Shane and Cronin, 2024). Such factors could impact the accuracy of the P-T estimates obtained through the Ridolfi (2021) thermobarometer, as it is calibrated for equilibrium conditions. However, the observed match between depth estimates from the amphibole compositions and regional geophysical data (Gao et al., 2021) provides a component of validation for the results, despite the potential complexity introduced by disequilibrium effects. This indicates that, while the amphibole-derived P-T estimates have the potential to capture depth of storage under equilibrium conditions, additional influences beyond P-T control should also be considered in interpreting these types of data.

## 6.2. Interpretation of amphibole breakdown textures

Amphibole breakdown textures commonly form due to decompression, heating, and late-stage oxidation processes, depending on mineral-melt characteristics such as composition, viscosity, water content, temperature, and pressure (Browne and Gardner, 2006; De Angelis et al., 2015; D’Mello et al., 2021; Rutherford and Devine, 2003; Rutherford and Hill, 1993). Experimental studies suggest that reaction (or breakdown) rims form when amphibole experiences magmatic conditions outside of its stability field (Browne and Gardner, 2006; Rutherford and Devine, 2003). For instance, while amphibole is stable and does not typically develop reaction rims if formed at depths greater than 100–110 MPa or shallower than 10 MPa, reaction rims do still have the potential to form if crystals come into contact with surrounding melt and experience a decrease in dissolved water content and pressure (Browne and Gardner, 2006). In this scenario, reaction rim growth occurs from the crystal edge inwards and develops only when in contact with a surrounding melt; rims will not develop when in contact with other crystals in the absence of melt (Browne and Gardner, 2006). The grain size of the rims can also be correlated with the time spent out of the amphibole stability field. For example, relatively fine-grained, thin rims can develop due to stalling at shallow depths, while relatively coarser-grained, equant and thicker rims can develop due to stalling at deeper levels within the magmatic system (Browne and Gardner, 2006). Various reaction rims and breakdown mechanisms have been discussed

in the literature based on texture and composition (Garcia and Jacobson, 1979; Murphy et al., 2000; Rutherford and Devine, 2003; Plechov et al., 2008; D’Mello et al., 2021). The four types of breakdown reactions within the Quillacas amphiboles and their associated formation processes, as informed by the work of Plechov et al. (2008) and D’Mello et al. (2021), are: 1) detached pyroxene rims - pyroxene microlites surround amphibole crystals and form due to a minor, but significant, temperature increase within the amphibole’s stability field (Fig. 6); 2) symplectic rims - intergrown streams of submicron mineral aggregates form due to ascent-driven decompression (Fig. 6); 3) granular rims - plagioclase, pyroxene, and oxides in zones of varying proportions, which form due to bi-metasomatic reaction between amphibole and melt (Fig. 6); 4) irregular volumetric decomposition - regions within the amphibole that are replaced by unaligned anhydrous mineral aggregates of plagioclase, clinopyroxene, and oxides due to isobaric heating (Fig. 7). Amphibole reaction rim thickness has also been proposed as a proxy for the time of heating and/or the timescales associated with magma ascent when considered within the context of experimental calibrations of rim width as a function of constant-rate decompression (Browne and Gardner, 2006; Rutherford and Devine, 2003; Rutherford and Hill, 1993). The evaluation of magma ascent pathways is however more comprehensive when reaction rim textures, thicknesses, and mineralogy are collectively considered, as they provide insights into the time spent outside of the amphibole stability field and the potential stalling depths within the magmatic system (Browne and Gardner, 2006). We therefore now consider these features in the context of breakdown mechanisms occurring within the Quillacas magmatic system and the process(es) that led to their formation.

Textural evidence within the amphibole population of the cumulate hornblendites is interpreted here to record multiple stages of crystallization and storage within the Quillacas magmatic system. The euhedral-subhedral nature of the cumulate tschermakites indicates crystallization in a relatively undisturbed magmatic environment at upper-crustal depths between 18 and 22 km, where tschermakitic amphibole compositions are stable (tschermakite is stable between 10 and 50 km, e.g., Cho and Ernst, 1991; Najorka et al., 2002). However, the cumulate tschermakites are ubiquitously surrounded by coarse-grained, granular reaction rims (Fig. 3a, 6a; Velázquez Santana et al., 2020). The granular reaction rim formation is attributed to breakdown due to melt-crystal interactions given that no rim formation is observed in areas where

the crystal boundary is not in contact with a melt (D’Mello et al., 2021). Their formation is consistent with the mechanism proposed by Plechov et al. (2008) resulting in a sequence of zones defined by pyroxene + plagioclase + Ti-magnetite in contact with the amphibole, followed by a pyroxene + plagioclase zone, and a pyroxene zone (detached rim) in contact with a melt (Fig. 6a). Consequently, to develop the granular rims, melt had to be present in the system and cool relatively slowly to facilitate the development of the coarse-grained, granular rims observed in the hornblendites. Furthermore, the presence of detached rims and regions of irregular volumetric decomposition within these cumulate amphiboles can be attributed to heating due to new melt injection into a magma storage reservoir at depth. This implies that both primary crystallization and subsequent storage of the hornblendites occurred at upper crustal depths (18–22 km) prior to their entrainment and eruption within the andesitic host Quillacas lavas.

The Quillacas andesites also host a tschermakite population that, in contrast to the cumulate tschermakites, exhibit thin, fine-grained reaction rims. These rims are predominantly symplectic with some intergrowth between symplectic and granular also observed (Fig. 6b-d). The striking contrast in the tschermakite reaction rim textures, but the near-equivalent chemical compositions of these two tschermakite populations, is difficult to reconcile without considering a mafic recharge or magma mixing event. Therefore, it is suggested that the andesite tschermakites began to crystallize during a recharge event into the upper crustal hornblendite cumulate reservoir. The presence of symplectic and granular rim intergrowth in the andesite amphibole population could also imply that the formation of both rim types is due to a magmatic reaction of an unstable amphibole and not a product of late-stage post-eruptive oxidation (D’Mello et al., 2021). Evidence for this is recorded in the lack of rim formation when the crystal is not in contact with the melt (Fig. 7e-f). Since reactions rims are suggested to form starting from the crystal edges and progressing inward, this implies that the symplectic rims formed prior to the granular rims. Therefore, the intergrowth of symplectic and granular rims in the andesite amphiboles likely indicates multi-stage cooling where andesite amphiboles initially cooled relatively faster, developing the symplectic rims. Once cooling slowed, melt pockets formed around these rims and allowed for the development of the granular rim zone (D’Mello et al., 2021). It is also possible that symplectic rim growth in the andesite amphiboles occurred during magma ascent towards the hornblendite cumulate reservoir and the granular rim zones were developed after cooling rates decreased. Evidence for the ascent-driven formation of the symplectic rims is seen in the acicular habit, high aspect ratios of the tschermakite crystals, and their fine-grained nature (Fig. 6b-d; Browne and Gardner, 2006). The andesite tschermakites record rim widths that are significantly thinner than those of the hornblendite tschermakites (Fig. 6f-g). The differences in the reaction rim thickness between the hornblendite (avg. 27.25  $\mu\text{m}$ ) and andesite (7–9  $\mu\text{m}$ ) amphiboles indicate that despite their similar initial growth histories (similar P-T conditions of amphibole crystallization), there are striking differences in the late-stage processes, particularly in their cooling histories. These two populations of unique reaction rim thicknesses likely imply that the evolution of the Quillacas magmatic system involved multiple storage periods and mixing of magmas ascending at different rates that then erupted together (D’Mello et al., 2021; McCanta et al., 2007). This process, through which multiple amphibole rim populations exist within a single magmatic system, has been widely documented in a range of other volcanic settings including small volume, intraplate settings (Nicholis and Rutherford, 2004) to large volume active margin settings (Athanasopoulos, 1997; Cashman and McConnell, 2005; Devine et al., 1998a, 1998b; McCanta et al., 2007; Nakagawa et al., 1998; Rutherford and Hill, 1993).

### 6.3. Rare earth element (REE) variations in amphibole populations

The observed differences in REE concentrations between amphiboles in the Quillacas andesites and those in the hornblendites likely reflect

the distinct magmatic environments and crystallization sequences of these two lithologies (Fig. 5). Amphiboles within the andesite host lavas are interpreted to have crystallized later during the magmatic evolution of the Quillacas system, from a more fractionated melt that was progressively enriched in incompatible elements (including REEs) as differentiation advanced. This enrichment process led to higher REE concentrations, especially in the LREEs, in the andesitic amphiboles relative to the hornblendites, which crystallized at an earlier stage from a less evolved, relatively REE-poor melt. Furthermore, the hornblendite cumulates are interpreted to have formed under relatively closed conditions which limited their exposure to more fractionated melts. In contrast, amphiboles in the andesites possibly crystallized in an open system setting where ongoing magma differentiation or recharge could further influence the melt composition prior to amphibole crystallization. Consequently, the relative LREE-enrichment and slightly wider range of Eu anomaly values observed in the andesites may reflect these processes. Variable plagioclase fractionation is also interpreted to contribute to all the observed negative Eu anomalies.

### 6.4. A petrogenetic model for the Quillacas magmatic system

Our petrogenetic model for the Quillacas magmatic system synthesizes textural, geothermobarometric, and geochemical data to outline the crystallization conditions and magmatic processes that formed the tschermakite amphiboles (Fig. 10). These tschermakites crystallized under relatively consistent P-T conditions ( $448\text{--}598 \pm 12$  % MPa and  $928\text{--}1004 \pm 22$  °C), corresponding to depths of 16–24 km within the Central Andean continental crust. The major element chemistry of amphiboles in both the host andesite and entrained hornblendite cumulates points to a common melt source region. However, REE concentrations reveal differences between the two amphibole populations. The hornblendite amphiboles suggest closed-system crystallization from a relatively REE-poor melt, while the andesite amphiboles reflect crystallization from a more evolved, potentially open-system melt.

Textural evidence further supports this magmatic evolution within the Quillacas system. As is evidenced by their large crystal size and euhedral nature, the hornblendite cumulate amphiboles likely crystallized first at upper crustal depths where they remained relatively stable. The injection of fresh magma into this storage zone then destabilized the hornblendite amphiboles and initiated a reaction with the new melt. This reaction produced the detached rims, which in viscous melts, can further develop into either symplectic or granular rims based on cooling rates (D’Mello et al., 2021). In the case of the hornblendite amphiboles, a slower cooling rate led to the formation of the granular rims. This recharge event also led to the crystallization of the andesite amphiboles. The andesite amphiboles then began developing symplectic rims due to a relatively fast cooling rate in an unstable environment as evidenced by their small crystal size and acicular habit. Once magma ascent began, the hornblendite and andesite tschermakites were collectively entrained in the melt which led to further destabilization and the development of volumetric decomposition. The absence of amphiboles with exclusively granular rims in the andesite samples suggests that the hornblendite cumulates either remained mostly solid during subsequent magma intrusion, preventing the entrainment of cumulate amphiboles into the andesites, or that magma ascent occurred relatively quickly.

This model highlights the broader significance of hornblendites in arc magmatic systems. As cumulate bodies within the arc crust, the hornblendites provide insights into processes of crustal differentiation and storage at various depths (e.g., Davidson et al., 2007), with their stability potentially reflecting periods of quiescence followed by reactivation upon recharge. Furthermore, it also underscores the complexity of magmatic systems in what is traditionally considered a monogenetic volcano. Monogenetic volcanoes are typically characterized by a single eruptive episode within a defined period with no temporal break in eruptive activity (Németh and Kereszturi, 2015; Smith and Németh, 2017). However, the term “monogenetic” can be limiting, as the

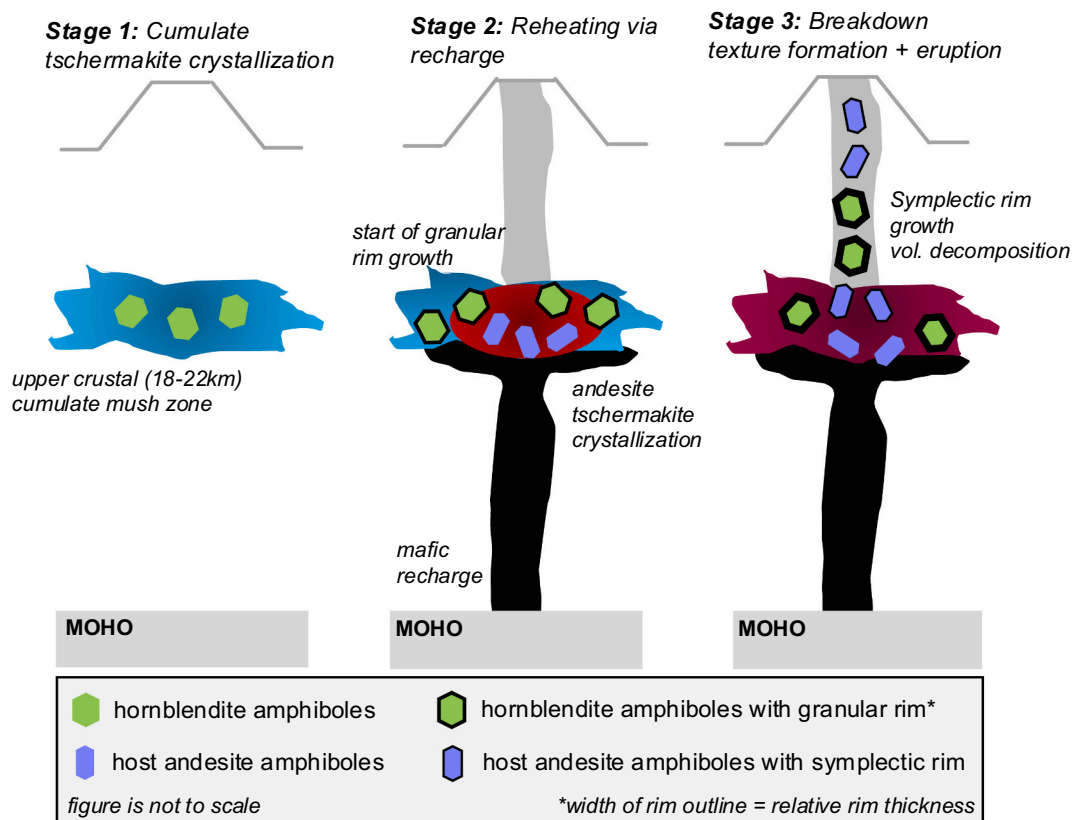


**Fig. 10.** Schematic petrogenetic model for the Quillacas magmatic system highlighting the inferred magma storage zone at upper crustal depths and petrogenesis of the amphibole populations as informed by textural, geochemical, and thermobarometric constraints.

eruptive products of monogenetic volcanoes often record evidence of complex plumbing systems (Coote et al., 2018; Gao et al., 2017; Larrea et al., 2023; Needham et al., 2011; Smith and Németh, 2017). Studies of crystal cargoes in monogenetic centers have suggested that processes such as stalling and crystallization may be more prevalent than the traditional model of rapid magma ascent from the mantle (Coote et al., 2018; Gao et al., 2017). Consistent with this emerging narrative, our study of the Quillacas monogenetic volcanic center reveals amphibole breakdown textures that are indicative of complex magmatic processes, including magma storage and stalling, decompression, and recharge. This observed complexity could suggest a continuum between geochemically monogenetic and polygenetic volcanic systems (Smith and Németh, 2017). Our study demonstrates the utility of amphibole as a recorder of mineralogical, textural, geochemical, and thermobarometric processes in magmatic systems at monogenetic systems. These findings underscore the complexity of volcanic systems, from monogenetic to polygenetic, and emphasize the need for detailed petrogenetic models to fully understand volcanic evolution and eruptive behavior across scales.

## 7. Conclusions

The study of the monogenetic Quillacas monogenetic volcanic center on the Eastern Bolivian Altiplano, Central Andes, documents the complex magmatic processes associated with amphibole fractionation throughout the arc crust and the utility of amphibole in deciphering magmatic processes. The combined data demonstrate that:

- (1) Amphiboles in the Quillacas magmatic system crystallized under tightly constrained P-T conditions ( $928\text{--}1004 \pm 22$  °C and  $448\text{--}598 \pm 12$  % MPa), corresponding to depths of 16–24 km in the upper continental crust. These results are consistent with a

low seismic velocity zone within this region of the Central Andean crust (Gao et al., 2021).

- (2) Amphibole breakdown textures, such as detached pyroxene rims, symplectic rims, granular rims, and irregular volumetric decomposition are common in the Quillacas amphiboles. These textures indicate multiple stages of crystallization, cooling, and recharge within the Quillacas magmatic system.
- (3) Differences in rare earth element (REE) concentrations between amphiboles in the andesites and hornblendites reflect crystallization at different evolutionary stages of the magmatic system. Andesite amphiboles show higher LREE concentrations when compared to the amphiboles in the hornblendites. This suggests that the hornblende amphibole crystallized first from a REE-poor melts while the andesite amphiboles crystallized later in the differentiation process from a more differentiated, incompatible element rich melt.
- (4) This study proposes a petrogenetic model in which hornblende amphiboles crystallize first in a cumulate mush zone at upper crustal depths. These hornblende amphiboles were then destabilized by a fresh magma injection which led to the development of detached and granular rims due to reheating. This melt also led to the crystallization of the andesite amphiboles. The development of symplectic rims in the andesite amphiboles is attributed to a combination of heating and decompression-induced degassing during ascent.
- (5) The Quillacas volcanic center challenges the traditional view of monogenetic volcanoes, showing evidence of complex magmatic processes, such as magma storage, stalling, decompression, and recharge. This complexity supports the idea of a continuum between monogenetic and polygenetic volcanic systems and emphasizes the need for detailed petrogenetic models to better understand volcanic evolution.

## CRedit authorship contribution statement

**L.C. Velázquez Santana:** Writing – review & editing, Writing – original draft, Visualization, Validation, Investigation, Formal analysis, Data curation, Conceptualization. **C.L. McLeod:** Writing – review & editing, Validation, Supervision, Resources, Project administration, Funding acquisition, Conceptualization. **B. Shaulis:** Writing – review & editing, Validation, Resources, Methodology. **M. Loocke:** Writing – review & editing, Validation, Resources, Methodology. **R. Al Gbory:** Visualization, Investigation, Funding acquisition.

## Declaration of competing interest

The authors declare that they have no known competing financial interests or personal relationships that could have appeared to influence the work reported in this paper.

## Data availability

Data are available through Mendeley Data at DOI:10.17632/45bhdjbdnf.2

## Acknowledgements

Matt Duley and Dr. Mark Krekeler are thanked for their training and support during the use of the SEM facility at the Miami University CAMI facility. Special thanks are extended to Jim and Susan Naus for financial support via the Naus Family Scholar Fund awarded to co-author McLeod which supported data acquisition via EPMA at Louisiana State University. Financial support was also provided via an Undergraduate Research Award from the Office of Research for Undergraduates at Miami University to co-author Al Gbory which supported LA-ICP-MS analyses at the University of Arkansas.

## Appendix A. Supplementary data

Supplementary data to this article can be found online at <https://doi.org/10.1016/j.lithos.2024.107891>.

## References

- Anderson, J.L., Smith, D.R., 1995. The effects of temperature and fO<sub>2</sub> on the Al-hornblende barometer. *Am. Mineral.* 80, 549–559. <https://doi.org/10.2138/am-1995-5-614>.
- Athanasopoulos, P., 1997. *The Origin and Ascent History of the 1996 Dacitic Dome, Volcan Popocatepetl, Mexico*. B.Sc. thesis. University of Manitoba, Winnipeg, p. 105.
- Barber, N.D., Edmonds, M., Jenner, F., Audétat, A., Williams, H., 2021. Amphibole control on copper systematics in arcs: Insights from the analysis of global datasets. *Geochim. Cosmochim. Acta* 307, 192–211. <https://doi.org/10.1016/j.gca.2021.05.034>.
- Barboni, M., Boehnke, P., Schmitt, A.K., Harrison, T.M., Shane, P., Bouvier, A.-S., Baumgartner, L., 2016. Warm storage for arc magmas. *Proc. Natl. Acad. Sci.* 113, 13959–13964. <https://doi.org/10.1073/pnas.1616129113>.
- Beck, S.L., Zandt, G., 2002. The nature of orogenic crust in the Central Andes. *J. Geophys. Res. Solid Earth* 107, 7–16. <https://doi.org/10.1029/2000JB000124>.
- Browne, B.L., Gardner, J.E., 2006. The influence of magma ascent path on the texture, mineralogy, and formation of hornblende reaction rims. *Earth Planet. Sci. Lett.* 246, 161–176. <https://doi.org/10.1016/j.epsl.2006.05.006>.
- Buckley, V.J.E., Sparks, R.S.J., Wood, B.J., 2006. Hornblende dehydration reactions during magma ascent at Soufrière Hills Volcano, Montserrat. *Contrib. Mineral. Petrol.* 151, 121–140. <https://doi.org/10.1007/s00410-005-0060-5>.
- Cashman, K.V., McConnell, S.M., 2005. Multiple levels of magma storage during the 1980 summer eruptions of Mount St. Helens, WA. *Bull. Volcanol.* 68, 57–75. <https://doi.org/10.1007/s00445-005-0422-x>.
- Cashman, K.V., Sparks, R.S.J., Blundy, J.D., 2017. Vertically extensive and unstable magmatic systems: a unified view of igneous processes. *Science* 355, eaag3055. <https://doi.org/10.1126/science.aag3055>.
- Cho, M., Ernst, W.G., 1991. An experimental determination of calcic amphibole solid solution along the join tremolite-tschermakite. *Am. Mineral.* 76, 985–1001.
- Cladouhos, T.T., Allmendinger, R.W., Coira, B., Farrar, E., 1994. Late cenozoic deformation in the Central Andes: fault kinematics from the northern Puna, northwestern Argentina and southwestern Bolivia. *J. South Am. Earth Sci.* 7, 209–228. [https://doi.org/10.1016/0895-9811\(94\)90008-6](https://doi.org/10.1016/0895-9811(94)90008-6).
- Cooper, K.M., 2019. Time scales and temperatures of crystal storage in magma reservoirs: implications for magma reservoir dynamics. *Philos. Trans. R. Soc. A Math. Phys. Eng. Sci.* 377, 20180009. <https://doi.org/10.1098/rsta.2018.0009>.
- Coote, A., Shane, P., Stirling, C., Reid, M., 2018. The origin of plagioclase phenocrysts in basalts from continental monogenetic volcanoes of the Kaikohe-Bay of Islands field, New Zealand: implications for magmatic assembly and ascent. *Contrib. Mineral. Petrol.* 173, 14. <https://doi.org/10.1007/s00410-018-1440-y>.
- Davidson, J., Turner, S., Handley, H., Macpherson, C., Dosseto, A., 2007. Amphibole “sponge” in arc crust? *Geology* 35, 787–790. <https://doi.org/10.1130/G23637A.1>.
- Davidson, J.P., de Silva, S.L., 1992. Volcanic rocks from the Bolivian Altiplano: Insights into crustal structure, contamination, and magma genesis in the Central Andes. *Geology* 20, 1127–1130. [https://doi.org/10.1130/0091-7613\(1992\)020<1127:VRFTBA>2.3.CO;2](https://doi.org/10.1130/0091-7613(1992)020<1127:VRFTBA>2.3.CO;2).
- Davidson, J.P., de Silva, S.L., 1995. Late Cenozoic magmatism of the Bolivian Altiplano. *Contrib. Mineral. Petrol.* 119, 387–408. <https://doi.org/10.1007/BF00286937>.
- Davidson, J.P., Hora, J.M., Garrison, J.M., Dungan, M.A., 2005. Crustal forensics in arc magmas. *J. Volcanol. Geothermal Res. Energy Mass Fluxes Volcanic Arcs* 140, 157–170. <https://doi.org/10.1016/j.jvolgeores.2004.07.019>.
- De Angelis, S.H., Larsen, J., Coombs, M., Dunn, A., Hayden, L., 2015. Amphibole reaction rims as a record of pre-eruptive magmatic heating: an experimental approach. *Earth Planet. Sci. Lett.* 426, 235–245. <https://doi.org/10.1016/j.epsl.2015.06.051>.
- Dessimo, M., Müntener, O., Ulmer, P., 2012. A case for hornblende dominated fractionation of arc magmas: the Chelan complex (Washington Cascades). *Contrib. Mineral. Petrol.* 163, 567–589. <https://doi.org/10.1007/s00410-011-0685-5>.
- Devine, J.D., Murphy, M.D., Rutherford, M.J., Barclay, J., Sparks, R.S.J., Carroll, M.R., Young, S.R., Gardner, J.E., 1998a. Petrologic evidence for pre-eruptive pressure-temperature conditions, and recent reheating, of andesitic magma erupting at the Soufrière Hills Volcano, Montserrat, W.I. *Geophys. Res. Lett.* 25, 3669–3672. <https://doi.org/10.1029/98GL01330>.
- Devine, J.D., Rutherford, M.J., Gardner, J.E., 1998b. Petrologic determination of ascent rates for the 1995–1997 Soufrière Hills Volcano andesitic magma. *Geophys. Res. Lett.* 25, 3673–3676. <https://doi.org/10.1029/98GL00912>.
- D’Mello, N.G., Zellmer, G.F., Negrini, M., Kereszturi, G., Procter, J., Stewart, R., Prior, D., Usuki, M., Iizuka, Y., 2021. Deciphering magma storage and ascent processes of Taranaki, New Zealand, from the complexity of amphibole breakdown textures. *Lithos* 398–399, 106264. <https://doi.org/10.1016/j.lithos.2021.106264>.
- Ganne, J., Bachmann, O., Feng, X., 2018. Deep into magma plumbing systems: Interrogating the crystal cargo of volcanic deposits. *Geology* 46, 415–418. <https://doi.org/10.1130/G39857.1>.
- Gao, R., Lassiter, J.C., Ramirez, G., 2017. Origin of temporal compositional trends in monogenetic vent eruptions: Insights from the crystal cargo in the Papoose Canyon sequence, big Pine Volcanic Field, CA. *Earth Planet. Sci. Lett.* 457, 227–237. <https://doi.org/10.1016/j.epsl.2016.10.013>.
- Gao, Y., Tilmann, F., van Herwaarden, D.-P., Thrastarson, S., Fichtner, A., Heit, B., Yuan, X., Schurr, B., 2021. Full waveform inversion beneath the Central Andes: insight into the dehydration of the nazca slab and delamination of the back-arc lithosphere. *J. Geophys. Res. Solid Earth* 126, e2021JB021984. <https://doi.org/10.1029/2021JB021984>.
- Garcia, M.O., Jacobson, S.S., 1979. Crystal clots, amphibole fractionation and the evolution of calc-alkaline magmas. *Contrib. Mineral. Petrol.* 69, 319–327. <https://doi.org/10.1007/BF00372257>.
- Göğüş, O.H., Sundell, K., Uluocak, E.Ş., Saylor, J., Çetiner, U., 2022. Rapid surface uplift and crustal flow in the Central Andes (southern Peru) controlled by lithospheric drip dynamics. *Sci. Rep.* 12, 5500. <https://doi.org/10.1038/s41598-022-08629-8>.
- Hammarstrom, J.M., Zen, E., 1986. Aluminum in hornblende: an empirical igneous geobarometer. *Am. Mineral.* 71, 1297–1313.
- Helz, R.T., 1982. Chapter 2, Experimental studies of amphibole stability; phase relations and compositions of amphiboles produced in studies of the melting behavior of rocks. *Rev. Mineral. Geochem.* 9B, 279–353.
- Humphreys, M.C.S., Blundy, J.D., Sparks, R.S.J., 2006. Magma evolution and open-system processes at Shiveluch volcano: insights from phenocryst zoning. *J. Petrol.* 47, 2303–2334. <https://doi.org/10.1093/petrology/egl045>.
- Jackson, M.D., Blundy, J., Sparks, R.S.J., 2018. Chemical differentiation, cold storage and remobilization of magma in the Earth’s crust. *Nature* 564, 405–409. <https://doi.org/10.1038/s41586-018-0746-2>.
- Kent, A.J.R., Darr, C., Koleszar, A.M., Salisbury, M.J., Cooper, K.M., 2010. Preferential eruption of andesitic magmas through recharge filtering. *Nature Geosci.* 3, 631–636. <https://doi.org/10.1038/ngeo924>.
- Kiss, B., Harangi, S., Ntaflou, T., Mason, P.R.D., Pál-Molnár, E., 2014. Amphibole perspective to unravel pre-eruptive processes and conditions in volcanic plumbing systems beneath intermediate arc volcanoes: a case study from Ciomadul volcano (SE Carpathians). *Contrib. Mineral. Petrol.* 167, 986. <https://doi.org/10.1007/s00410-014-0986-6>.
- Krawczynski, M.J., Grove, T.L., Behrens, H., 2012. Amphibole stability in primitive arc magmas: effects of temperature, H<sub>2</sub>O content, and oxygen fugacity. *Contrib. Mineral. Petrol.* 164, 317–339. <https://doi.org/10.1007/s00410-012-0740-x>.
- Kuno, H., 1950. Petrology of Hakone volcano and the adjacent areas, JAPAN. *GSA Bulletin* 61, 957–1020. [https://doi.org/10.1130/0016-7606\(1950\)61\[957:POHVAT\]2.0.CO;2](https://doi.org/10.1130/0016-7606(1950)61[957:POHVAT]2.0.CO;2).
- Larrea, P., Widom, E., Siebe, C., Salinas, S., Kuentz, D., 2023. Deciphering the sources and processes feeding young monogenetic volcanoes from the Michoacán Guanajuato Volcanic Field (Mexico): a study case of El Astillero and El Pedregal. *Lithos* 456–457, 107302. <https://doi.org/10.1016/j.lithos.2023.107302>.
- Leake, B.E., Woolley, A.R., Arps, C.E.S., Birch, W.D., Gilbert, M.C., Grice, J.D., Hawthorne, F.C., Kato, A., Kisch, H.J., Krivovichev, V.G., Linthout, K., Laird, J., Mandarino, J., Maresch, W.V., Nickel, E.H., Rock, N.M.S., Schumacher, J.C.,

- Smith, D.C., Stephenson, N.C.N., Ungaretti, L., Whittaker, E.J.W., Youzhi, G., 1997. Nomenclature of amphiboles; report of the subcommittee on amphiboles of the international mineralogical association commission on new minerals and mineral names. *Mineral. Mag.* 61, 295–310. <https://doi.org/10.1180/minmag.1997.061.405.13>.
- Li, L., Xiong, X.L., Liu, X.C., 2017. Nb/Ta fractionation by amphibole in hydrous basaltic systems: implications for arc magma evolution and continental crust formation. *J. Petrol.* 58, 3–28. <https://doi.org/10.1093/ptrology/egw070>.
- Luo, C.-H., Wang, R., Nebel, O., Li, Q.-W., 2024. Amphibole fractionation as a key driver for oxidation of magmas in convergent margins. *Earth Planet. Sci. Lett.* 641, 118851. <https://doi.org/10.1016/j.epsl.2024.118851>.
- Marrett, R., Emerman, S.H., 1992. The relations between faulting and mafic magmatism in the Altiplano-Puna plateau (Central Andes). *Earth Planet. Sci. Lett.* 112, 53–59. [https://doi.org/10.1016/0012-821X\(92\)90006-H](https://doi.org/10.1016/0012-821X(92)90006-H).
- Marsh, B.D., 2006. Dynamics of magmatic systems. *Elements* 2, 287–292. <https://doi.org/10.2113/gselements.2.5.287>.
- McCanta, M.C., Rutherford, M.J., Hammer, J.E., 2007. Pre-eruptive and syn-eruptive conditions in the Black Butte, California dacite: Insight into crystallization kinetics in a silicic magma system. *J. Volcanol. Geotherm. Res.* 160, 263–284. <https://doi.org/10.1016/j.jvolgeores.2006.10.004>.
- McLeod, C.L., Davidson, J.P., Nowell, G.M., de Silva, S.L., 2012. Disequilibrium melting during crustal anatexis and implications for modeling open magmatic systems. *Geology* 40, 435–438. <https://doi.org/10.1130/G33000.1>.
- McLeod, C.L., Davidson, J.P., Nowell, G.M., de Silva, S.L., Schmitt, A.K., 2013. Characterizing the continental basement of the Central Andes: Constraints from Bolivian crustal xenoliths. *GSA Bull.* 125, 985–997. <https://doi.org/10.1130/B30721.1>.
- Mégard, F., Noble, D.C., Mckee, E.H., Bellon, H., 1984. Multiple pulses of Neogene compressive deformation in the Ayacucho intermontane basin, Andes of Central Peru. *GSA Bulletin* 95, 1108–1117. [https://doi.org/10.1130/0016-7606\(1984\)95<1108:MPONCD>2.0.CO;2](https://doi.org/10.1130/0016-7606(1984)95<1108:MPONCD>2.0.CO;2).
- Molina, J.F., Moreno, J.A., Castro, A., Rodríguez, C., Fershtater, G.B., 2015. Calcic amphibole thermobarometry in metamorphic and igneous rocks: New calibrations based on plagioclase/amphibole Al-Si partitioning and amphibole/liquid Mg partitioning. *Lithos* 232, 286–305. <https://doi.org/10.1016/j.lithos.2015.06.027>.
- Murphy, M.D., Sparks, R.S.J., Barclay, J., Carroll, M.R., Brewer, T.S., 2000. Remobilization of andesite magma by intrusion of mafic magma at the soufrière hills volcano, Montserrat, West Indies. *Journal of Petrology* 41, 21–42. <https://doi.org/10.1093/ptrology/41.1.21>.
- Najorka, J., Gottschalk, M., Heinrich, W., 2002. Composition of synthetic tremolite-tschermakite solid solutions in amphibole + anorthite-and amphibole + zoisite-bearing assemblages. *Am. Mineral.* 87, 462–477. <https://doi.org/10.2138/am-2002-0410>.
- Nakagawa, M., Nairn, I.A., Kobayashi, T., 1998. The ~10 ka multiple vent pyroclastic eruption sequence at Tongariro Volcanic Centre, Taupo Volcanic Zone, New Zealand: part 2. Petrological insights into magma storage and transport during regional extension. *J. Volcanol. Geotherm. Res.* 86, 45–65. [https://doi.org/10.1016/S0377-0273\(98\)00086-9](https://doi.org/10.1016/S0377-0273(98)00086-9).
- Nakamura, N., 1974. Determination of REE, Ba, Fe, Mg, Na and K in carbonaceous and ordinary chondrites. *Geochim. Cosmochim. Acta* 38, 757–775. [https://doi.org/10.1016/0016-7037\(74\)90149-5](https://doi.org/10.1016/0016-7037(74)90149-5).
- Needham, A.J., Lindsay, J.M., Smith, I.E.M., Augustinus, P., Shane, P.A., 2011. Sequential eruption of alkaline and sub-alkaline magmas from a small monogenetic volcano in the Auckland Volcanic Field, New Zealand. *J. Volcanol. Geotherm. Res.* 201, 126–142. <https://doi.org/10.1016/j.jvolgeores.2010.07.017>.
- Németh, K., Kereszturi, G., 2015. Monogenetic volcanism: personal views and discussion. *Int. J. Earth Sci. (Geol. Rundsch)* 104, 2131–2146. <https://doi.org/10.1007/s00531-015-1243-6>.
- Nicholis, M.G., Rutherford, M.J., 2004. Experimental constraints on magma ascent rate for the Crater flat volcanic zone hawaiiite. *Geology* 32, 489–492. <https://doi.org/10.1130/G20324.1>.
- Pesquera, A., Gil-Crespo, P.P., 2024. Deciphering magmatic processes from plagioclase, clinopyroxene and amphibole chemistry and textures: a case study of a basaltic lava flow in the Basque-Cantabrian Basin (Northern Spain). *Miner. Petrol.* 118, 253–280. <https://doi.org/10.1007/s00710-024-00850-9>.
- Plechov, P.Yu., Tsai, A.E., Shcherbakov, V.D., Dirksen, O.V., 2008. Opacitization conditions of hornblende in Bezymyanni volcano andesites (March 30, 1956 eruption). *Petrology* 16, 19–35. <https://doi.org/10.1134/S0869591108010025>.
- Reubi, O., Blundy, J., 2009. A dearth of intermediate melts at subduction zone volcanoes and the petrogenesis of arc andesites. *Nature* 461, 1269–1273. <https://doi.org/10.1038/nature08510>.
- Ridolfi, F., 2021. Amp-TB2: an updated model for calcic amphibole thermobarometry. *Minerals* 11, 324. <https://doi.org/10.3390/min11030324>.
- Ridolfi, F., Renzulli, A., 2012. Calcic amphiboles in calc-alkaline and alkaline magmas: thermobarometric and chemometric empirical equations valid up to 1,130°C and 2.2 GPa. *Contrib. Mineral. Petrol.* 163, 877–895. <https://doi.org/10.1007/s00410-011-0704-6>.
- Rutherford, M.J., Devine, J.D., 2003. Magmatic Conditions and Magma Ascent as Indicated by Hornblende phase Equilibria and Reactions in the 1995–2002 Soufrière Hills Magma. *J. Petrol.* 44, 1433–1453. <https://doi.org/10.1093/ptrology/44.8.1433>.
- Rutherford, M.J., Hill, P.M., 1993. Magma ascent rates from amphibole breakdown: an experimental study applied to the 1980–1986 Mount St. Helens eruptions. *J. Geophys. Res. Solid Earth* 98, 19667–19685. <https://doi.org/10.1029/93JB01613>.
- Schaaf, P., Stimac, J., Siebe, C., Macías, J.L., 2005. Geochemical evidence for mantle origin and crustal processes in volcanic rocks from Popocatepetl and surrounding monogenetic volcanoes, Central Mexico. *J. Petrol.* 46, 1243–1282. <https://doi.org/10.1093/ptrology/egi015>.
- Schleicher, J.M., Bergantz, G.W., Breidenthal, R.E., Burgisser, A., 2016. Time scales of crystal mixing in magma mushes. *Geophys. Res. Lett.* 43, 1543–1550. <https://doi.org/10.1002/2015GL067372>.
- Shane, P., Cronin, S., 2024. Pre-eruptive magmatic processes at Taranaki volcano from an amphibole perspective. *J. Volcanol. Geotherm. Res.* 452, 108144. <https://doi.org/10.1016/j.jvolgeores.2024.108144>.
- Shane, P., Smith, V.C., 2013. Using amphibole crystals to reconstruct magma storage temperatures and pressures for the post-caldera collapse volcanism at Okataina volcano. *Lithos* 156–159, 159–170. <https://doi.org/10.1016/j.lithos.2012.11.008>.
- Smith, I.E.M., Németh, K., 2017. Source to surface model of monogenetic volcanism: a critical review. In: Németh, K., Carrasco-Núñez, G., Aranda-Gómez, J.J., Smith, I.E.M. (Eds.), *Monogenetic Volcanism*. Geological Society of London, p. 0. <https://doi.org/10.1144/SP446.14>.
- Straub, S.M., Gómez-Tuena, A., Vannucchi, P., 2020. Subduction erosion and arc volcanism. *Nat. Rev. Earth Environ.* 1, 574–589. <https://doi.org/10.1038/s43017-020-0095-1>.
- Sun, S.-s., McDonough, W.F., 1989. Chemical and isotopic systematics of oceanic basalts: implications for mantle composition and processes. *Geological Society, London, Special Publications* 42, 313–345. <https://doi.org/10.1144/GSL.SP.1989.042.01.19>.
- Svoboda, C., Rooney, T.O., Girard, G., Deering, C., 2022. Transcrustal magmatic systems: evidence from andesites of the southern Taupo Volcanic Zone. *J. Geol. Soc. London* 179, jgs2020-204. <https://doi.org/10.1144/jgs2020-204>.
- Szymanowski, D., Wotzlaf, J.-F., Ellis, B.S., Bachmann, O., Guillong, M., von Quadt, A., 2017. Protracted near-solidus storage and pre-eruptive rejuvenation of large magma reservoirs. *Nat. Geosci.* 10, 777–782. <https://doi.org/10.1038/ngeo3020>.
- Triantafyllou, A., Berger, J., Baele, J.-M., Mattioli, N., Ducea, M.N., Sterckx, S., Samson, S., Hodel, F., Ennih, N., 2020. Episodic magmatism during the growth of a Neoproterozoic oceanic arc (Anti-Atlas, Morocco). *Precambrian Res.* 339, 105610. <https://doi.org/10.1016/j.precamres.2020.105610>.
- Ureta, G., Aguilera, F., Németh, K., Inostroza, M., González, C., Zimmer, M., Menzies, A., 2020. Transition from small-volume ephemeral lava emission to explosive hydrovolcanism: the case of Cerro Tujle maar, northern Chile. *J. South Am. Earth Sci.* 104, 102885. <https://doi.org/10.1016/j.jsames.2020.102885>.
- Vargas-Arcila, L., Murcia, H., Osorio-Ocampo, S., Sánchez-Torres, L., Botero-Gómez, L.A., Bolaños, G., 2023. Effusive and evolved monogenetic volcanoes: two newly identified (~800 ka) cases near Manizales City, Colombia. *Bull. Volcanol.* 85, 42. <https://doi.org/10.1007/s00445-023-01655-y>.
- Velázquez Santana, L.C., McLeod, C.L., Blakemore, D., Shaulis, B., Hill, T., 2020. Bolivian hornblende cumulates: Insights into the depths of Central Andean arc magmatic systems. *Lithos* 370–371, 105618. <https://doi.org/10.1016/j.lithos.2020.105618>.
- Ward, K.M., Zandt, G., Beck, S.L., Wagner, L.S., Tavera, H., 2016. Lithospheric structure beneath the northern Central Andean Plateau from the joint inversion of ambient noise and earthquake-generated surface waves. *Journal of Geophysical Research: Solid Earth* 121, 8217–8238. <https://doi.org/10.1002/2016JB013237>.
- Wörner, G., Mamani, M., Blum-Oeste, M., 2018. Magmatism in the Central Andes. *Elements* 14, 237–244. <https://doi.org/10.2138/gselements.14.4.237>.
- Zandt, G., Velasco, A.A., Beck, S.L., 1994. Composition and thickness of the southern Altiplano crust, Bolivia. *Geology* 22, 1003–1006. [https://doi.org/10.1130/0091-7613\(1994\)022<1003:CATOTS>2.3.CO;2](https://doi.org/10.1130/0091-7613(1994)022<1003:CATOTS>2.3.CO;2).